Available online at www.sciencedirect.com

ScienceDirect

Energy Procedia 55 (2014) 361 – 368

Energy Procedia

4th International Conference on Silicon Photovoltaics, SiliconPV 2014

Two-level metallization and module integration of point-contacted solar cells

Henning Schulte-Huxel[a,*], Udo Römer[a], Susanne Blankemeyer[a], Agnes Merkle[a], Yevgeniya Larionova[a], Verena Steckenreiter[a], Robby Peibst[a], Sarah Kajari-Schroeder[a], Rolf Brendel[a,b]

[a]*Institute for Solar Energy Research Hamelin (ISFH), Am Ohrberg 1, D-31860 Emmerthal, Germany*
[b]*Institut für Festkörperphysik, Leibniz Universität Hannover, Appelstraße 2, D-30167 Hannover, Germany*

Abstract

We present a module integration process for back junction back contact (BJBC) solar cells featuring point contacts to the back surface field (BSF). We apply two metallization layers. A first metal layer of aluminum is deposited onto the rear side of the cell and carries the current extracted from the polarity with the larger surface area fraction, e.g. from the emitter. The second metallization layer is an Al layer on a transparent substrate that we laser-weld to the small and point-shaped regions of the other polarity, e.g. the BSF region. We use a polymer for insulation between the two metal layers. The Al layer on the substrate also serves for cell interconnection, i.e., it enables module integration. Such an interconnection structure halves the fill factor losses due to the metallization. First proof-of-principle modules show a shunt free interconnection, no laser-induced damage, and an energy conversion efficiency of up to 20.7%.

Peer-review under responsibility of the scientific committee of the SiliconPV 2014 conference

Keywords: laser micro welding; module integration; cell interconnection; Al metallization; back junction back contact; point contact solar cells

* Corresponding author. Tel.: +49-5151-999-303; fax: +49-5151-999-400.
E-mail address: h.schulte@isfh.de

Peer-review under responsibility of the scientific committee of the SiliconPV 2014 conference
doi:10.1016/j.egypro.2014.08.104

1. Introduction

Back junction back contact (BJBC) solar cells are one of the most promising high-efficiency solar cells concepts. Solar cells reaching 24% efficiency have been developed by different groups [1–4]. Among many others, geometrical aspects are still an issue. For reaching high efficiencies it is favorable:

(i) to minimize the area of the back surface field (BSF) since this reduces electrical shading [5],
(ii) to have a short distance between adjacent BSF regions for small lateral transport losses [6],
(iii) and to have equally large cross sections of the metal contacts for both polarities for low metal resistance losses [7,8].

Point-shaped BSF regions [4,9] resolve the first aspect. The second aspect can be addressed by a sufficiently small BSF pitch. The reduction of the resistive losses in the metallization is achieved by decoupling the geometry of the metallization from the doping geometry. The decoupling requires insulating dielectric layers. Ensuring a high insulation on large area is known to be challenging with commonly used passivation layers [4,7,10].

Two-level metallization, also called multilevel metallization, allows for large metal cross sections of both polarities [11] since the full rear side area rather than individual fingers are utilized for current transport. Up to now, two-level metallization requires complex processing: deposition of the first metal layer, contact separation, application of a stack of insulation layers (e.g. like anodic oxidized Al and SiOx), opening of the dielectric layers on the point contacts, deposition of the second metal layer and finally the module integration of the cells [11]. Thus, an enabling technology for a realization of two-level metallization is still missing. We present a process adapted to point-contact solar cells based on a laser welding process. It combines the significant reduction in series resistance of the two-level metallization with a slim module integration process sequence.

2. Simultaneous two-level metallization and module integration

Our technique realizes a two-level metallization as well as module integration. We use evaporated Al on the solar cell´s rear side as the first metal layer. The evaporated Al-contacts of both polarities on the cell rear side are separated, leaving isolated metal pads on the point-shaped BSF regions and a continuous metallization on the emitter region. An Al layer on a transparent substrate serves as the second metallization layer. The Al layer on the substrate is simultaneously used as the interconnection for module integration.

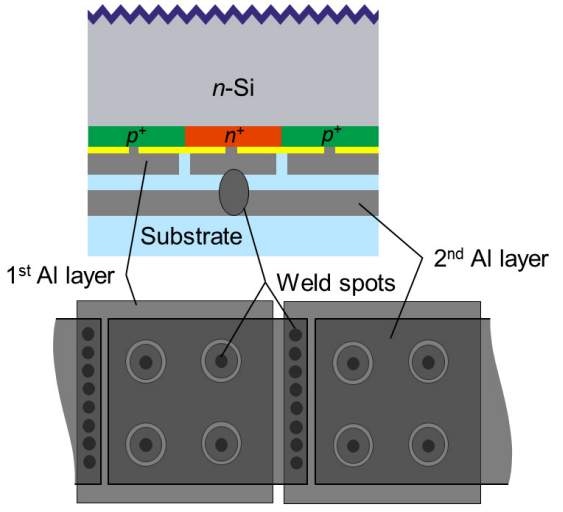

Fig. 1. Schematic of two-level metallization. The first Al layer, which carries the current of the p^+ emitter regions, is directly deposited on the cell, the second is deposited on a transparent substrate. The n^+ BSF regions are contacted to the second Al layer by laser welding.

Figure 1 schematically depicts the concept of the two-level metallization enabled by laser welding. For insulation between the first and second Al layer, a liquid polymer that is identical to the lamination material is deposited and cured under ambient conditions on the whole rear side of the solar cell. The contact between the isolated metal pads contacting the BSF in the first layer and the Al layer on the substrate is created by the aluminum-based mechanical and electrical laser interconnection (AMELI) process [12]. This laser welding process penetrates through the polymer layer. Thus, no separate processing of via openings is required. After the laser welding process, ribbons for external connection are welded to the Al layer. For the final lamination we use an encapsulant film and a front glass or foil.

As a proof of principle, two types of modules are fabricated:

Type 1: One solar cell (50 × 50 mm²) with circular BSF (Ø 400 µm) contacts. The emitter and BSF contacts are in the same plane (no height difference), as shown in Fig.1. This cell is interconnected on a glass substrate metallized with 10 µm evaporated Al. The contacting of the emitter metallization for interconnection is realized by straight busbars on two edges. The busbars are about 1 mm wide.

Type 2: Two solar cells (25 × 125 mm²) with rectangular BSF contacts (570 ×620 µm²) and an index of 1600 µm. Figure 2 left side schematically depicts the geometry of the doping. The cell rear side features a height difference of 20 µm between the emitter region and the BSF contacts (the latter protrude from the cell rear side). The cell interconnection is realized via an Al foil with an interdigitated structure (Fig. 2 right side). An encapsulant film is used as substrate carrying a 10-µm-thick structured Al-foil.

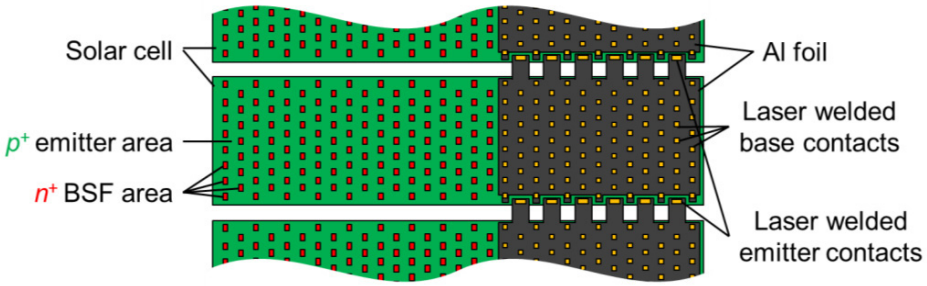

Fig. 2. Scheme of the interconnection process with three cells of type 2. The green and red areas indicate the emitter and base regions, respectively. The laser welded areas are shown in yellow and the Al foil in grey.

Due to the non-continuous base metallization, the solar cells cannot be measured prior to interconnection. The measurements after interconnection are performed without a shadow mask. Please note that the cells themselves are not optimized.

3. Results

3.1 Solar cells type 1 on glass substrate

Table 1 shows the *I-V*-characteristics of the module 1 fabricated on glass. The interconnected solar cell has an open circuit voltage V_{oc} of 668 mV and an efficiency of 20.6%. After lamination the open circuit voltage is unchanged within the measurement uncertainty. Please note that reflection at the front side of the glass, multiple reflections within the module and other optical effects may have an impact after lamination leading to a change in the short circuit current density J_{sc}. Since the values before laser welding are not accessible, the impacts of the interconnection have to be determined by other techniques.

Table 1. *I-V*-characteristics of the proof-of-principle module 1 consisting of one 50 mm × 50 mm-sized cell. The efficiency is related to the cell area *A*.

	A (cm²)	V_{oc} (mV)	J_{sc} (mA/cm²)	FF (%)	η (%)
Before lamination	25	668	40.6	75.9	20.6
After lamination	25	668	41.0	74.8	20.4

For the module integration based on laser welding it is crucial that no laser damage is induced and that the polymer layer insulates well to avoid local shunts. Therefore, we perform infrared light modulated lock-in thermography (ILIT) measurements [13,14]. Figure 3 a) shows the ILIT image of module 1 after interconnection. An increase in signal can be observed at the laser diced, non-passivated edges. This laser damage leads to increased recombination, which can reduce the current and should be minimized. However, in the center, where the laser welding is applied, no shunts can be observed. This shows that no local shunts due to insufficient insulation between the metal layers are induced. Since the open circuit voltage V_{oc} measured on the final module corresponds to the implied open circuit voltage $V_{oc,impl.}$ measured by QSSPC on the cell precursor prior to metallization, we conclude that no laser damage is induced by the interconnection process.

A third requirement is a homogeneous contacting of all BSF points to collect the generated current. Fig. 3 b) and c) show the electroluminescence (EL) images of module type 1 after laser welding and after final lamination, respectively. Inhomogeneous regions with reduced EL intensity can be resolved. These regions are obviously caused by an imperfect contacting rather than by an increased non-radiative recombination path, since they are not visible in ILIT images. We attribute these few poor-contacted regions to particles present on the sample prior to laser welding, leading to an increased spacing between the cell and the metallized glass. This would result in a locally increased contact resistance. The rather low fill factor of module 1 is caused by this issue. Obviously, counteractions against particles (filtered air, nitrogen blowing) on the cells are required during the interconnection process for the proposed module interconnection scheme. In contrast to this the high J_{sc} of 40.6 mA/cm² shows an effective current collection.

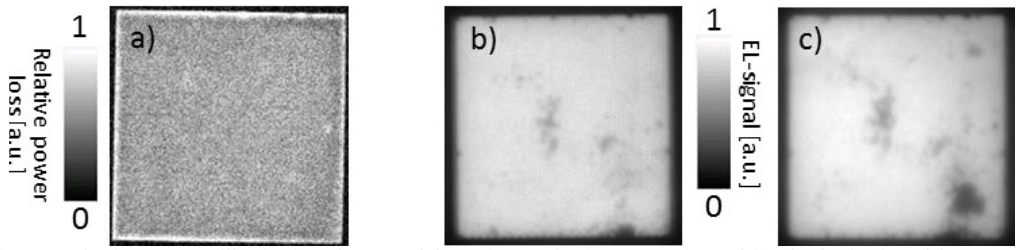

Fig. 3. (a) ILIT cosine images at an illumination of 1 sun and (b) EL image after interconnection and (c) after lamination of the contacted cell at an applied voltage of 0.7 V of module type 1. The images are in linear scale.

3.2 Solar cells type 2 on encapsulant film substrate

To avoid inhomogeneous contacting due to particles or not planar interfaces, we substitute the rigid glass substrate (as reported in Sec. 3.1) by a flexible substrate on basis of a lamination foil metallized with an Al foil. Two solar cells of type 2 are connected in series to demonstrate the interconnection. Table 2 shows the I-V-characteristics of the module consisting of the two cells.

Table 2. *I-V*-characteristics of the proof-of-principle module 2 consisting of two 25 mm × 125 mm-sized cells. The efficiency is related to the cell area *A*.

	A (cm²)	V_{oc} (mV)	J_{sc} (mA/cm²)	FF (%)	η (%)
Before lamination	62.5	1350	20.16	76.0	20.7
After lamination	62.5	1343	19.7	70.2	18.6

The results show the successful contacting and interconnection of both point-contact cells. An open circuit voltage V_{oc} of 1350 mV is achieved, which corresponds to an average open circuit voltage of 675 mV for each cell. The rather high open circuit voltage indicates that the laser interconnection does not induce significant damage. The efficiency of the module related to the cell area is 20.7%. The short circuit current density J_{sc} of the module of 20.16 mA/cm² corresponds to a short circuit current density J_{sc} on cell level of 40.3 mA/cm².

In order to detect possible shunts we again performed ILIT measurements. The figures 4 a) and b) show the ILIT images of the solar cells before interconnection. The edges of the cells have an increased signal, indicating locally increased non-radiative recombination paths. Further features are the labeling of the cells on the right edges and features originating from handling in the central area. An ILIT image of the interconnected cells is presented in Fig. 4 c). It shows the same features as prior to interconnection. We do not observe localized shunts, e. g. from an insufficient insulation of the two Al layers.

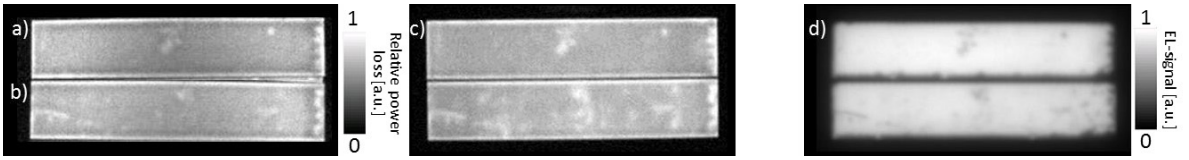

Fig. 4. (a) and (b) ILIT cosine images of the cells before and (c) after interconnection at an illumination of 1 sun. (d) EL image of the contacted cells at an applied voltage of 1.35 V. The images are in linear scale.

Figure 4 d) shows an EL image of the interconnected cells that reveals the features also apparent in the ILIT images. No additional areas with reduced signal are observed in the central area of the cell. This indicates a reliable contact to all BSF points. Only at the lower positioned edges of the cells, where the interdigitated interconnector is located (see Fig. 2), some BSF points are not contacted.

After lamination one cell is locally shunted at an edge where the Al foil touches the first metallization layer. This could be avoided by leaving the outer edges of the solar cell rear side non-metallized.

4. Reduction of series resistance by AMELI two-level metallization

So far, we have demonstrated the simplified two level metallization process. Besides the advantage of a decoupling of the geometries of doped areas and metallization (see above), our two-level metallization concept has the potential for a further reduction of the metallization-induced part of the series resistance. In case of a "conventional" interdigitated back contact (IBC)structure with one metallization layer and equal wide fingers, only the half of the area is available for current conduction for each polarity. In case of the two-level metallization, the whole area, except the area of the point contacts, can be used for current conduction of one polarity. The current of the second polarity is conducted in the Al-foil, which is also as wide as the cell.

To estimate the advantage of the two-level metallization scheme, we determine the area weighted resistance in the finger in the case of linearly increasing current by [15]

$$R_s = \frac{1}{3}\rho\frac{i\,l_F^2}{A_F} \tag{1}$$

with i being the index width of the fingers, lF the length of the fingers, which is here equal to the cell width, and AF the cross-section area of the fingers perpendicular to the direction of the current transport. The metal coverage of the rear side is 95%, the resistivity of the evaporated Al ρevap = 3.2 μΩ·cm [16] and for the Al-foil ρbulk = 2.7 μΩ·cm [17]. The thickness of each Al layer is 10 μm. These thicknesses of Al cell metallization can be deposited in industrial tools with high throughput [18]. The contributions by the conductive layers/fingers carrying the current of base and emitter are added up. Since in the case of two-layer metallization two 10-μm-thick Al layers conduct the current, in a rough approximation the resistance is reduced by a factor of two. For more detailed calculation we take into account the different resistivities of the Al layers and that the Al foil covers 100% of the rear side.

Since an increase in area weighted series resistance Rs leads in first approximation to a reduction of the voltage,

the reduction of the fill factor ΔFF can be approximated by

$$\Delta FF = \frac{\Delta V_{mpp} \cdot J_{mpp}}{V_{oc} \cdot J_{sc}} = \frac{\Delta R_S \cdot J_{mpp}^2}{V_{oc} \cdot J_{sc}}. \quad (2)$$

To show the impact of the reduced series resistance we take as a rough estimation Jmpp = 38 mA/cm², Jsc = 41 mA/cm² and Voc = 680 mV. Fig. 5 shows the resulting series resistance and fill factor losses for both cases as a function of the finger length lF (equivalent to the cell width). The two-level metallization leads to a reduction of the series resistance by a factor of 2.2 for all sizes of solar cells compared to a conventional one-level IBC metallization. In case of full area 15.6 cm × 15.6 cm large solar cells, the contribution of the finger metallization to the series resistance are 1092 mΩ·cm² (488 mΩ·cm²) for an IBC cell (for our two-level metallization). The latter still corresponds to a significant resistive power loss. Increasing the metal thickness further seems not feasible regarding process throughput and wafer bow. However, the series resistance could be reduced to an acceptable value of Rs = 116 mΩ·cm² for a halved solar cell interconnected by the two-level metallization. The resulting fill factor loss induced by the metallization in this case would be 0.6% absolute, which is a significant reduction compared to the 1.3% absolute in case of an IBC solar cell. Furthermore, conventional IBC solar cells have busbars which lead to additional series resistance in the metallization as well as in the base material [19].

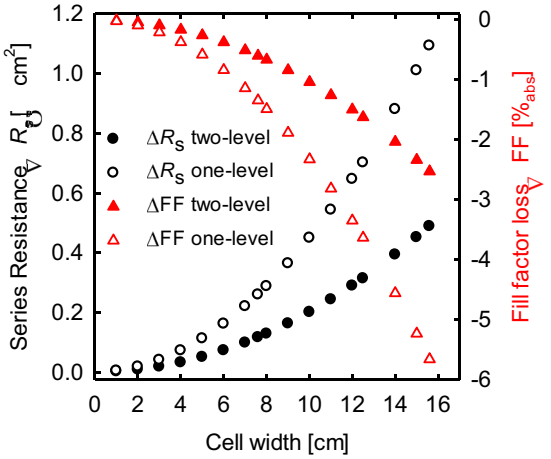

Fig. 5. Series resistance contributions (circles, black) and fill factor losses (triangles, red) for a one-level IBC concept (open symbols) and the two-level metallization (closed symbols). Note that the contribution of the busbar metallization, which might be significant in case of the one-layer concept, is not taken into account here.

5. Conclusion

The doping geometry of point-contacted BJBC solar cells offers the possibility to maximize the current collection and minimize the series resistance due to lateral charge carrier transport in the base material. Nevertheless, for standard interconnection using busbars the metallization geometry needs to be different from the doping geometry. This leads to challenges in insulation. Here we demonstrate a module interconnection process, which allows to contact a metallization scheme being equal to the underlying doping scheme. This is achieved by laser welding an Al foil to the individual BSF point contacts using the AMELI process. Due to the high accuracy of today's laser systems structures in the order of 100 µm can be contacted. In this scheme the Al-foil carries the base current, whereas the metal layer on the cell carries the emitter current. The same Al-foil serves also as the interconnect device for module integration of the point-contacted solar cells. As insulation layer between the two metal levels we

use a thin film of encapsulation material instead of a dielectric stack of vacuum deposited oxides. The encapsulant film is deposited and cured under ambient conditions. The properties of the insulation layer (e.g. pin holes or cracks) are less critical in the case of an Al foil compared to a second Al layer which is evaporated.

We demonstrated our simplified process for a two-level metallization of point-contacted solar cells and their simultaneous module interconnection by two proof-of-principle modules with different types of solar cells. Both modules show a shunt free interconnection by laser welding proving the insulation quality of the polymer film. The EL images show the contacting of the BSF contact points, which enable the collection of the current generated in the solar cells. Efficiency up to 20.7% has been demonstrated. The presented process is capable to contact solar cells featuring contacts protruding the rear side, which can result from the definition of the base and emitter regions, as well as solar cells with a planar rear side.

The process reduces the series resistance of the metallization by a factor of 2.2 compared to conventional IBC solar cells. However, an interconnection of full area 15.6 cm × 15.6 cm large solar cells seems still to induce a rather high series resistance of 488 mΩ·cm², even for an Al thickness of 10 µm. This value can be reduced to 116 mΩ·cm² when slicing one wafer into two half cells.

Acknowledgements

The authors thank Ilka Feilhaber, Heike Kohlenberg and Sarah Spätlich for cell processing as well as Tobias Neubert and David Sylla for laser support. This work was supported by the German Ministry for the Environment, Nature Conservation, and Reactor Safety under Contract 0325192 (CrystalLine Project) and the State of Lower Saxony.

References

[1] Cousins PJ, Smith DD, Luan H, Manning J, Dennis TD, Waldhauer A, Wilson KE, Harley G, Mulligan WP. Generation 3: Improved performance at lower cost. Proc. 35th IEEE PVSC 2010:275–278.

[2] Blakers A, Fong K, Franklin E, Grant N, Wan Y, Wnag D, Zin S, Kho T, McIntosh K. 24.6% efficient back contact cell with oxide - nitride passivation. Proc. 23rd Int. PVSEC 2013.

[3] Nakamura J, Kimoto K, Asano N, Hieda T, Koide N, Katayama HFY, Nakamura K. Development of Hetero-Junction Back Contact Si Solar Cells toward the conversion efficiency of 25%. Proc. 23rd Int. PVSEC 2013.

[4] Reichel C, Granek F, Hermle M, Glunz SW. Back-contacted back-junction n -type silicon solar cells featuring an insulating thin film for decoupling charge carrier collection and metallization geometry. Prog. Photovolt: Res. Appl. 2013;21(5):1063–1076.

[5] Hermle M, Granek F, Schultz-Wittmann O, Glunz SW. Shading Effects in Back-Junction Back-Contacted Silicon Solar Cells. Proc. 33rd IEEE PVSC 2008:412–415.

[6] Granek F, Hermle M, Huljić DM, Schultz-Wittmann O, Glunz SW. Enhanced lateral current transport via the front N + diffused layer of n-type high-efficiency back-junction back-contact silicon solar cells. Prog. Photovolt: Res. Appl. 2009;17(1):47–56.

[7] Robbelein J, Vermang B, Janssens T, Posthuma NPJ. Passivation Layers for Large Area Interdigitated Back Junction Cells and Their Electrical Isolation Properties. Proc. 26th EU PVSEC 2011:1008–1013.

[8] Harder N, Mertens V, Brendel R. Buried emitter solar cell structures: Decoupling of metallisation geometry and carrier collection geometry of back contacted solar cells. phys. stat. sol. (RRL) 2008;2(4):148–150.

[9] Swanson R, Beckwith S, Crane R, Eades W, Young Hoon Kwark, Sinton R, Swirhun S. Point-contact silicon solar cells. IEEE Trans. Electron Devices 1984;31(5):661–664.

[10] Keding R, Bock R, Bochow A, Katkhouda K, Stüwe D, Reichel C, Clement F, Woehl R, Reinecke H, Geppert T. Study of the Electrical Insulation of Dielectric Passivation Layers and Stacks for Back-Contact Back-Junction Silicon Solar Cells. Proc. 28th EU PVSEC 2013: 961–966.

[11] Verlinden P, Swanson R, Sinton R, Kane D. Multilevel metallization for large area point-contact solar cells. Proc. 20th IEEE PVSC 1988:532–537.

[12] Schulte-Huxel H, Blankemeyer S, Bock R, Merkle A, Kajari-Schröder S, Brendel R. Al-Foil on Encapsulant for the Interconnection of Al-Metalized Silicon Solar Cells. IEEE J. Photovoltaics 2013;3(1):77–82.

[13] Kaes M, Seren S, Pernau T, Hahn G. Light-modulated lock-in thermography for photosensitivepn-structures and solar cells. Prog. Photovolt: Res. Appl. 2004;12(5):355–363.

[14] Kasemann M, Walter B, Meinhardt C, Ebser J, Kwapil W, Warta W. Emissivity-corrected power loss calibration for lock-in thermography measurements on silicon solar cells. J. Appl. Phys. 2008;103(11):113503.

[15] Green MA. Silicon solar cells: Advanced principles & practice. Sydney: Centre for Photovoltaic Devices and Systems Univ. of New South Wales; 1995.

[16] Nekarda J, Reinwand D, Grohe A, Hartmann P, Preu R, Trassl R, Wieder R. Industrial PVD metallization for high efficiency crystalline silicon solar cells. Proc. 34th IEEE PVSC 2009:892–896.
[17] Vargel C. Corrosion of aluminium. 1st ed. Amsterdam, Boston: Elsevier; 2004.
[18] Mader C, Müller J, Eidelloth S, Brendel R. Local rear contacts to silicon solar cells by in-line high-rate evaporation of aluminum. Solar Energy Materials and Solar Cells 2012;107:272–282.
[19] Schulte-Huxel H, Blankemeyer S, Merkle A, Steckenreiter V, Kajari-Schroeder S, Harder N, Brendel R. Interconnection of busbar-free back contacted solar cells by laser welding. Prog. Photovolt: Res. Appl. 2014:submitted.